

# Photonic crystal fibers confining light by both index-guiding and bandgap-guiding: hybrid PCFs

Limin Xiao, Wei Jin, M.S. Demokan

Department of Electrical Engineering, The Hong Kong Polytechnic University, Kowloon, Hong Kong, China  
[xiaolimin.ee@polyu.edu.hk](mailto:xiaolimin.ee@polyu.edu.hk)

**Abstract:** We propose two kinds of hybrid photonic crystal fiber (PCF) structures and investigate the properties of such PCFs in detail. The modal effective index, mode field area, confinement loss, group velocity dispersion, and birefringence are numerically simulated and compared with those of the corresponding index-guiding and bandgap PCFs, which allows for a deeper understanding of the guiding mechanism of the hybrid PCFs. The advantages of hybrid PCFs and potential applications are also discussed.

©2007 Optical Society of America

**OCIS codes:** (060.2310) Fiber optics; (060.5295) Photonic crystal fibers.

---

## References and links

1. J. C. Knight, T. A. Birks, P. St. J. Russell, and D. M. Atkin, "All-silica single-mode optical fiber with photonic crystal cladding," *Opt. Lett.* **21**, 1547-1549 (1996).
2. J. C. Knight, J. Broeng, T. A. Birks, and P. St. J. Russell, "Photonic band gap guidance in optical fibers," *Science* **282**, 1476-1478 (1998).
3. T. A. Birks, J. C. Knight, and P. S. J. Russell, "Endlessly single-mode photonic crystal fiber," *Opt. Lett.* **22**, 961-963 (1997).
4. J. C. Knight, T. A. Birks, R. F. Cregan, P. S. J. Russell and P. D de Sandro, "Large mode area photonic crystal fibre," *Electron. Lett.* **34**, 1347-1348 (1998).
5. W. Wadsworth, R. Percival, G. Bouwmans, J. Knight, and P. Russell, "High power air-clad photonic crystal fibre laser," *Opt. Express* **11**, 48-53 (2003). <http://www.opticsinfobase.org/abstract.cfm?URI=oe-11-1-48>
6. A. Ortigosa-Blanch, J. C. Knight, W. J. Wadsworth, J. Arriaga, B. J. Mangan, T. A. Birks, and P. S. J. Russell, "Highly birefringent photonic crystal fibers," *Opt. Lett.* **25**, 1325-1327 (2000)
7. P. Petropoulos, T. M. Monro, W. Belardi, K. Furusawa, J. H. Lee, and D. J. Richardson, "2R-regenerative all-optical switch based on a highly nonlinear holey fiber," *Opt. Lett.* **26**, 1233-1235 (2001).
8. T. A. Birks, D. Mogilevtsev, J. C. Knight, and P. St. J. Russell, "Dispersion compensation using single-material fibers," *IEEE Photon. Technol. Lett.* **11**, 674-676 (1999).
9. C. M. Smith, N. Venkataraman, M. T. Gallagher, D. Müller, J. A. West, N. F. Borrelli, D. C. Allan and K. W. Koch, "Low-loss hollow-core silica/air photonic bandgap fibre," *Nature* **424**, 657-659 (2003).
10. F. Luan, A. K. George, T. D. Hedley, G. J. Pearce, D. M. Bird, J. C. Knight, and P. S. J. Russell, "All-solid photonic bandgap fiber," *Opt. Lett.* **29**, 2369-2371 (2004)
11. B. Eggleton, C. Kerbage, P. Westbrook, R. Windeler, and A. Hale, "Microstructured optical fiber devices," *Opt. Express* **9**, 698-713 (2001) <http://www.opticsinfobase.org/abstract.cfm?URI=oe-9-13-698>
12. B. Temelkuran, S. D. Hart, G. Benoit, J. D. Joannopoulos, and Y. Fink, "Wavelength-scalable hollow optical fibres with large photonic bandgaps for CO<sub>2</sub> laser transmission," *Nature* **420**, 650-653 (2002).
13. S.G. Johnson, S. Fan, P.R. Villeneuve, J. D. Joannopoulos, and L.A. Kolodziejski, "Guided modes in photonic-crystal slabs," *Phys. Rev. B* **60**, 5751-5780 (1999).
14. A. Cerqueira S. Jr., F. Luan, C. M. B. Cordeiro, A. K. George, and J. C. Knight, "Hybrid photonic crystal fiber," *Opt. Express* **14**, 926-931 (2006). <http://www.opticsinfobase.org/abstract.cfm?URI=oe-14-2-926>
15. T. A. Birks, P. J. Roberts, P. St. J. Russell, D. M. Atkin, T. J. Shepherd, "Full 2-D photonic bandgaps in silica/air structures," *Electron. Lett.* **31**, 1941-1942 (1995).
16. N. Litchinitser, S. Dunn, B. Usner, B. Eggleton, T. White, R. McPhedran, and C. de Sterke, "Resonances in microstructured optical waveguides," *Opt. Express* **11**, 1243-1251 (2003). <http://www.opticsinfobase.org/abstract.cfm?URI=oe-11-10-1243>
17. S. Guo and S. Albin, "Simple plane wave implementation for photonic crystal calculations," *Opt. Express* **11**, 167-175 (2003). <http://www.opticsinfobase.org/abstract.cfm?URI=oe-11-2-167>
18. M. Koshiba, "Full vector analysis of photonic crystal fibers using the finite element method," *IEICE Electron. E85-C* **4**, 881-888 (2002).
19. K. Saitoh and M. Koshiba, "Numerical modeling of photonic crystal fibers," *J. Lightwave Technol.* **23**, 3580-3580 (2005).

20. K. Saitoh and M. Koshiba, "Leakage loss and group velocity dispersion in air-core photonic bandgap fibers," *Opt. Express* **11**, 3100-3109 (2003). <http://www.opticsinfobase.org/abstract.cfm?URI=oe-11-23-3100>
21. K. Saitoh and M. Koshiba, "Full-vectorial imaginary-distance beam propagation method based on finite element scheme: Application to photonic crystal fibers," *IEEE J. Quantum Electron.* **38**, 927-933 (2002).
22. N. A. Mortensen, "Effective area of photonic crystal fibers," *Opt. Express* **10**, 341-348 (2002) <http://www.opticsinfobase.org/abstract.cfm?URI=oe-10-7-341>
23. K. Nielsen, D. Noordegraaf, T. Sørensen, A. Bjarklev, and T. P. Hansen, "Selective filling of photonic crystal fibres," *J. Opt. A: Pure Appl. Opt.* **7**, L13-L20 (2005).
24. L. Xiao, W. Jin, M. Demokan, H. Ho, Y. Hoo, and C. Zhao, "Fabrication of selective injection microstructured optical fibers with a conventional fusion splicer," *Opt. Express* **13**, 9014-9022 (2005) <http://www.opticsinfobase.org/abstract.cfm?URI=oe-13-22-9014>
25. S. D. Hart, G. R. Maskaly, B. Temelkuran, P. H. Pridaux, J. D. Joannopoulos, and Y. Fink, "External reflection from omnidirectional dielectric mirror fibers," *Science* **296**, 510-513 (2002).
26. P. J. A. Sazio, A. Amezcua-Correa, C. E. Finlayson, J. R. Hayes, T. J. Scheidemantel, N. F. Baril, B. R. Jackson, D.-J. Won, F. Zhang, E. R. Margine, V. Gopalan, V. H. Crespi, and J. V. Badding, "Microstructured Optical Fibers as High-Pressure Microfluidic Reactors," *Science* **311**, 1583-1586 (2006).
27. A. Argyros, T. Birks, S. Leon-Saval, C. M. Cordeiro, F. Luan, and P. S. J. Russell, "Photonic bandgap with an index step of one percent," *Opt. Express* **13**, 309-314 (2005). <http://www.opticsinfobase.org/abstract.cfm?URI=oe-13-1-309>

---

## 1. Introduction

Photonic crystal fibers (PCFs) [1, 2], as a new class of fibers, have been investigated with great interest for a number of years. PCFs generally guide light by two different guiding mechanisms: index-guiding [1] or bandgap-guiding [2]. In index-guiding PCFs, similar to conventional fibers, light is guided in a higher index core by modified total internal reflection from a low effective index cladding; in bandgap PCFs, light is confined in a low-index core by reflection from a photonic crystal cladding. Because of their novel guiding mechanism and variety in design, PCFs have a number of novel properties and significant applications. For index-guiding PCFs, the properties include endlessly single mode [3], large mode area [4], high numerical aperture [5], high birefringence [6], high nonlinear coefficient [7] and dispersion management [8]. Various bandgap PCFs and many significant applications for them have been achieved, such as low-loss air-core bandgap PCFs [9], all-solid bandgap PCFs [10], a variety of PCF devices [11] and Bragg PCFs for CO<sub>2</sub> laser transmission [12].

Most PCFs guide light by only one of the two different guiding mechanisms, although hybrid-guiding (combination of index-guiding and bandgap-guiding) has been utilized in photonic crystal slabs [13] for many years. Recently, Cerqueira et al. [14] first demonstrated a hybrid PCF which guided light by both index-guiding and bandgap-guiding simultaneously. This hybrid PCF was composed of air holes and Ge-doped silica rods disposed around an undoped silica core; the air holes were arranged in a hexagonal pattern as in an index-guiding PCF, while the high index rods replaced a single row of air holes along one of the PCF axes. The authors mentioned that this hybrid PCF shared properties of both index-guiding and bandgap-guiding. However, the hybrid PCF is a quite new issue; although Cerqueira et al. proposed a kind of hybrid PCF and gave some basic analysis, it was not a systematic investigation that offers insight into the nature of the hybrid PCF, and many significant properties of hybrid PCFs have not been investigated.

In this paper, we propose two kinds of hybrid PCF structures and carry out detailed investigations on these hybrid PCFs. The modal effective index, effective mode area, confinement loss, group velocity dispersion and birefringence are theoretically investigated. The properties of hybrid PCFs are compared with those of the corresponding index-guiding PCF and bandgap-guiding PCF, which gives a physical insight into the guiding mechanism of the hybrid PCFs. Finally, the potential applications of these hybrid PCFs are discussed.

## 2. Description of the Approach

The guiding mechanism of an index-guiding PCF can be simply explained by the effective-index model [3], which is similar to light propagation in a traditional step-index fiber. The guiding mechanism of a bandgap PCF can be predicted by photonic bandgap theory [15], and

it also can be explained intuitively by antiresonant reflecting guidance [16]: light at wavelengths satisfying the antiresonant condition is guided in the core by antiresonant reflection from periodically placed high-index rods. Thus we can make an assumption that the light may propagate along the fiber when the light can be confined in the core by index-guiding in one direction and bandgap-guiding in the other direction in the transverse direction, even if the bandgap structure is not a full two dimensional photonic crystal structure.

The structure of a hybrid PCF is a modified PCF structure which is obtained by replacing one or more longitudinal sets of air holes of an air-silica index-guiding PCF by high-index rods as shown in Fig. 1, where black holes represent high-index rods and empty holes are air (or low-index) holes. In a hybrid PCF A, air holes are in the majority. In a hybrid PCF B, high-index rods are in majority. Of course there can be many other structures which can be devised by replacing different lines of hexagonal structure or changing the size of replacing holes/rods, which we do not illustrate in Fig. 1. Here we focus on investigating two categories of hybrid PCFs.

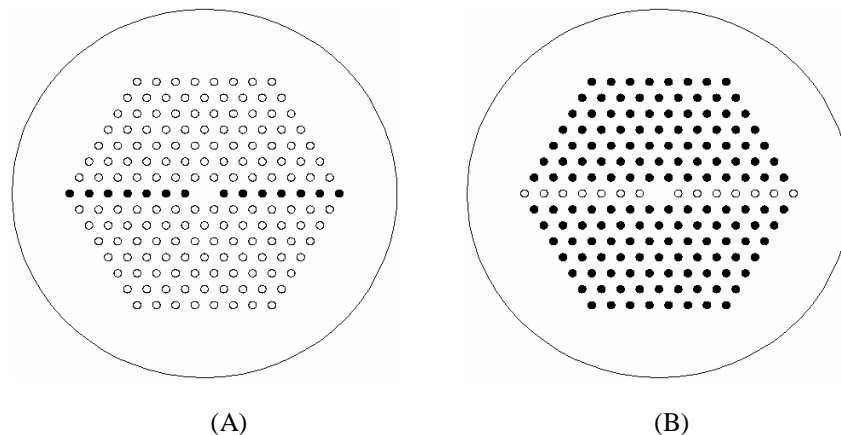


Fig. 1. Schematics of cross-sections of two kinds of hybrid PCFs, whereas black holes are high-index rods, empty holes are air holes.

In order to have a comprehensive understanding of the properties of the hybrid PCFs A and B, it is necessary to investigate the properties of the corresponding index-guiding PCF and bandgap PCF at the same time and compare the properties of the hybrid PCFs with them. In our simulations, the hybrid PCFs A and B have 7 rings of holes arranged in a hexagonal pattern, the PCFs have a pitch  $\Lambda$  of  $7.5 \mu\text{m}$  and a relative hole size  $d/\Lambda$  of 0.4. We assume that the background silica refractive index is 1.45, and the high-index rod has a refractive index of 1.48.

To analyze PCFs accurately, we use full-vector plane-wave method (PWM) [17] to calculate the bandgap map of the bandgap-guiding PCF and full-vector finite-element method (FEM) [18-20] to model the properties of all PCFs, including index-guiding, bandgap-guiding, hybrid-guiding A, hybrid-guiding B. Because of the structure symmetry of these PCFs, one quarter of the fiber cross section is investigated to calculate the modal effective indices in two orthogonal directions [18]. We also model the whole cross section of the fiber, which agrees well with the results from the quarter cross section. The cladding effective index of the fundamental space-filling mode is calculated by applying the full-vector FEM to an elementary piece of the index-guiding PCF cladding [18]. The effective mode area of a PCF,  $A_{\text{eff}}$ , is defined as [19]:

$$A_{eff} = \frac{(\iint_S |E_t|^2 dx dy)^2}{\iint_S |E_t|^4 dx dy} = \pi \omega^2 \quad (1)$$

where  $E_t$  is the transverse electric field vector and  $S$  denotes the whole fiber cross section.  $2\omega$  is mode field diameter (MFD) for a Gaussian shaped mode field distribution. The confinement loss  $L_c$  can be calculated by full-vector FEM with anisotropic perfectly matched layers (PMLs) [20, 21]:

$$L_c = 8.686\alpha \quad (2)$$

where  $\alpha$  is attenuation constant of the complex propagation constant. The unit of  $L_c$  is in decibels per meter. The group velocity dispersion (GVD),  $D_w$ , of a PCF can be deduced from [20]:

$$D_w = -\frac{\lambda}{c} \frac{d^2 n_{eff}}{d\lambda^2} \quad (3)$$

where  $n_{eff}$  is the wavelength dependent effective index,  $\lambda$  is the wavelength, and  $c$  is the velocity of light in vacuum. Material dispersion is neglected [20] in our simulations. The birefringence is defined as:

$$B = |n_{eff}^x - n_{eff}^y| \quad (4)$$

where  $n_{eff}^x$  and  $n_{eff}^y$  are the effective indices of the fundamental  $E_x$  mode and  $E_y$  mode respectively.

### 3. Analysis and Discussion

The wavelength range we considered is from 0.55  $\mu\text{m}$  to 2.1  $\mu\text{m}$ . For the index-guiding PCF and bandgap PCF, the fundamental modes of x-polarization and y-polarization are degenerate because of symmetry. However, for the hybrid PCF A and B, the fundamental modes are not degenerate because the guiding mechanisms in two orthogonal directions are different. For hybrid PCFs, we only consider the x-polarized fundamental mode in our simulations because the effective index difference of the two orthogonal fundamental modes is quite small in our cases. The difference will be discussed in section 3.5.

#### 3.1 Modal effective index

The light can be guided in the core of the index-guiding PCF when the effective index of the guided mode is larger than the cladding effective index and smaller than the refractive index of the core. For bandgap PCF, only when the modal effective index is within the bandgap regions and smaller than the core index, the light can be guided in the core. According to the resonance theory in Ref. [16], the cut-off wavelengths can be only determined by analyzing an individual high-index rod, which agree well with the bandgap edges predicted by bandgap theory. So we can assume that although the hybrid PCF does not have a full two-dimensional bandgap structure, the bandgap maps can also be approximately suitable for representing the hybrid PCF A and B. The hybrid PCF can guide the light only when the guiding conditions of both index-guiding and bandgap-guiding are satisfied.

As shown in the Fig. 2, the green line is the effective index of the fundamental mode of the index-guiding PCF and the red lines represent the effective indices of the bandgap PCF. The cladding line and silica line are the effective indices of the cladding and the core respectively. The solid black lines are the edges of the bandgap of the bandgap-guiding PCF. We can find from Fig. 2 that the light in the whole wavelength range can be well guided in the index-

guiding PCF, the effective index decreases gradually with the increase in wavelength. The bandgap PCF has three band gap regions in this range; the guided modes outside the bandgaps are cut off, thus light can propagate in three discrete transmission windows: about 1.26  $\mu\text{m}$  to 2.1  $\mu\text{m}$  in the first gap, 0.76  $\mu\text{m}$  to 1.18  $\mu\text{m}$  in the second gap and 0.55  $\mu\text{m}$  to 0.68  $\mu\text{m}$  in the third gap. The magnitude of the slope of the effective index curve of the bandgap PCF is larger than that of the index-guiding PCF. The crossing points of green line and red line are at the wavelengths about 0.57  $\mu\text{m}$ , 0.91  $\mu\text{m}$ , and 1.79  $\mu\text{m}$ . That means for these wavelengths, the guided modes have the same effective index even if the guiding mechanisms are different.

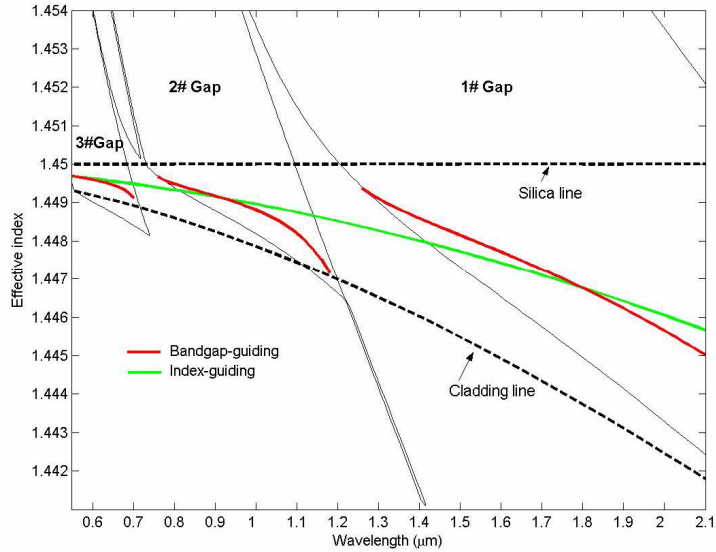


Fig. 2. Modal effective index of the fundamental modes and bandgap map as a function of wavelength.

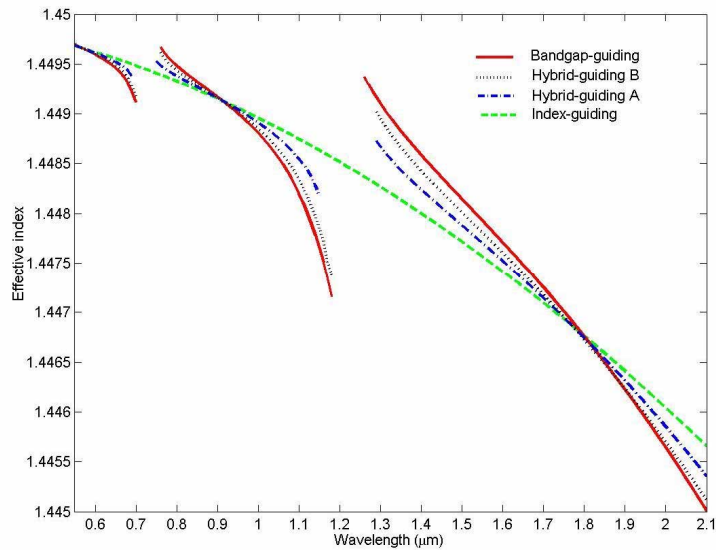


Fig. 3. Modal effective index of fundamental mode as a function of wavelength. The green dashed line is index-guiding PCF; the red solid line is bandgap PCF; the blue dash-dot line is hybrid PCF A and the black dotted line is hybrid PCF B.

The modal effective index of the hybrid PCFs A and B are shown in Fig. 3. We can find that the effective indices of hybrid PCFs are between the effective indices of the index-guiding PCF and bandgap PCF, and the hybrid PCF has the property of discrete frequency bands. This can be explained by the nature of hybrid-guiding. The hybrid PCF A confines light by bandgap effect in x direction and the hybrid PCF B confines light by bandgap effect in the cross-section except x direction. So the hybrid PCF should have properties of bandgap-guiding. The effective index curves of the hybrid PCF A are closer to the curve of index-guiding PCF compared with hybrid PCF B, and the effective index curves of hybrid PCF B are closer to the curve of bandgap PCF. This is because the index-guiding is the main guiding mechanism in hybrid PCF A and bandgap-guiding is the main guiding mechanism according to their refractive index distribution in the cross-section. The cross points of the curves of the four PCFs in Fig. 3 correspond to almost the same wavelengths as the cross points of index-guiding PCF and bandgap PCF shown in Fig. 2. That means if the effective index of index-guiding PCF and bandgap PCF is equivalent for one wavelength, the effective index of hybrid guiding PCF will have the same value at that wavelength, which proves again that the hybrid PCF guides light by a combination of both index-guiding and bandgap-guiding. It should be mentioned that in Ref. [14], the effective index curve of the hybrid PCF based on the preform A has an overlap with the curve of the index-guiding PCF for a range of wavelengths, that is because the refractive index of the high-index rod is a gradual variation, which cause the modal effective index of bandgap PCF to have an overlap with the index-guiding PCF, thus causing the overlap with the hybrid PCF.

### 3.2 Effective mode area

Effective mode area is an important parameter in investigating the modal properties; it has relevance to nonlinearity, confinement loss, bending loss, splicing loss and numerical aperture [22]. Fig. 4 shows the normalized effective mode area of different PCFs.

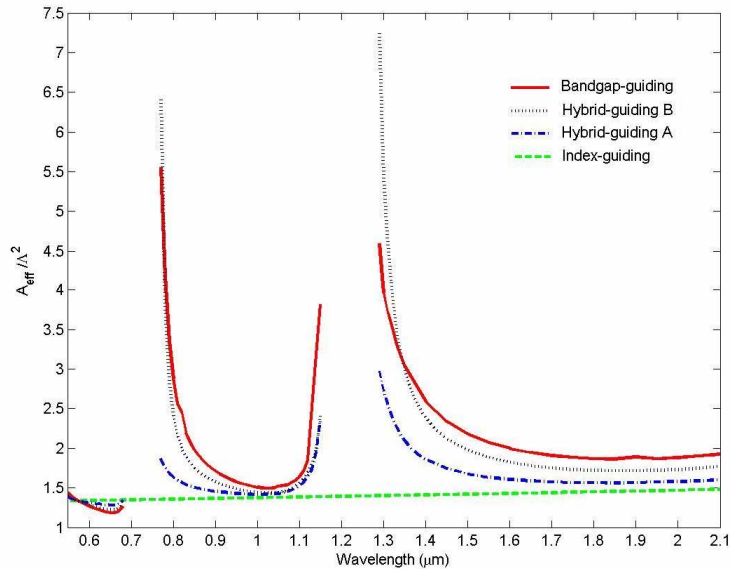


Fig. 4. Normalized effective mode area of the fundamental mode as a function of wavelength.

For the index-guiding PCF, the effective mode area increases very slowly with an increase in the wavelength. The MFD is  $9.78 \mu\text{m}$  at the wavelength  $0.55 \mu\text{m}$  and increases to  $10.30 \mu\text{m}$  at the wavelength  $2.10 \mu\text{m}$ , as shown in Fig. 5a(1-5) for the wavelength range from  $0.65 \mu\text{m}$  to  $1.55 \mu\text{m}$ . However, for the bandgap PCF, the effective mode area changes dramatically.

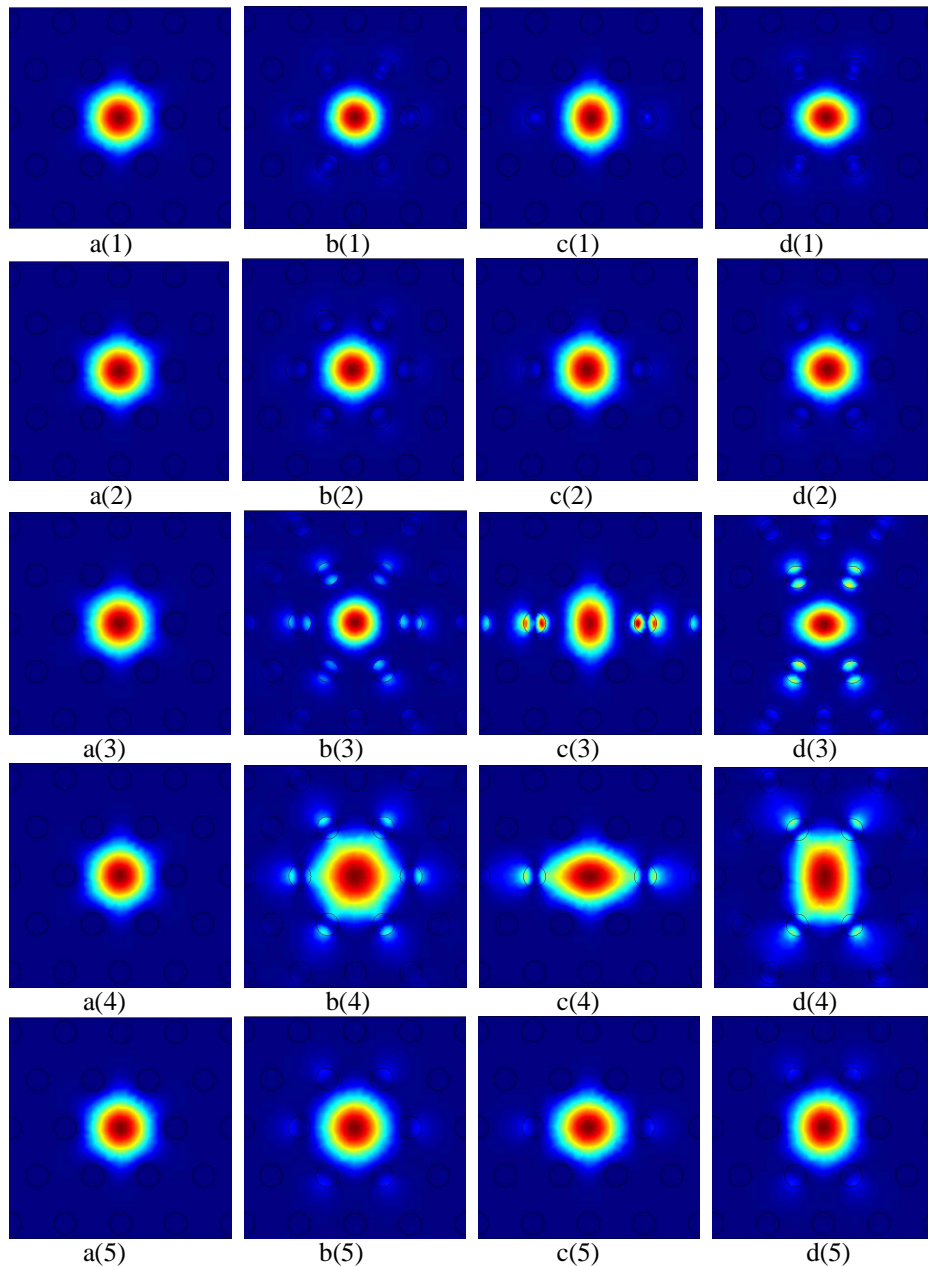


Fig. 5. Mode intensity distribution of fundamental modes of a (1-5) the index-guiding PCF, b(1-5) the bandgap PCF, c(1-5) the hybrid PCF A and d(1-5) the hybrid PCF B. The wavelength is (1) 0.65  $\mu\text{m}$ , (2) 1.0  $\mu\text{m}$ , (3) 1.15  $\mu\text{m}$ , (4) 1.30  $\mu\text{m}$  and (5) 1.55  $\mu\text{m}$ .

When the wavelengths of the light are close to the middle of the bandgap, the guided modes are well confined in the core, as shown in Fig. 5b(1, 2, 5). At the wavelength 0.65  $\mu\text{m}$  in the third bandgap (Fig. 5b(1)), the fundamental mode is well confined in the core, the MFD is 9.21  $\mu\text{m}$  which is smaller than the MFD of the index-guiding PCF (9.81  $\mu\text{m}$ ); at the wavelength 1.0  $\mu\text{m}$  in the second bandgap (Fig. 5b(2)), the MFD is 10.39  $\mu\text{m}$ , which is slightly larger than the MFD of index-guiding PCF (9.92  $\mu\text{m}$ ); at the wavelength 1.55  $\mu\text{m}$  in

the first bandgap (Fig. 5b(5)), the MFD is  $12.18\ \mu\text{m}$ , which is significantly larger than the MFD of index-guiding PCF ( $10.10\ \mu\text{m}$ ). When the wavelengths of the light are close to the edges of the bandgap, the effective mode area enlarges rapidly, as shown in Fig. 5b(3, 4). This is because of the resonance of the mode in the high-index rod with the core mode [16], which causes the mode to expand and thus increasing the leakage loss.

For the hybrid PCF A and B, the effective mode area is between the effective mode areas of the index-guiding PCF and bandgap PCF when the operation wavelengths are within the middle part of the bandgaps, as shown in Fig. 4. The effective mode area curve of hybrid PCF A is closer to that of index-guiding PCF and the effective mode area curve of hybrid PCF B is closer to that of the bandgap PCF. When the operation wavelengths are close to the middle of the bandgaps, the fundamental modes can be well-confined, as shown in Fig. 5c(1, 2, 5) and Fig. 5d(1, 2, 5). For example, at the wavelength  $0.65\ \mu\text{m}$ , the normalized mode areas of hybrid PCF A and B are 1.28 and 1.22 respectively, which is between that of the index-guiding PCF (1.34) and bandgap PCF (1.19). At the wavelength  $1.55\ \mu\text{m}$ , the normalized mode areas of the hybrid PCF A and B are 1.63 and 1.88 respectively, which is between that of the index-guiding PCF (1.42) and the bandgap PCF (2.07). When the operation wavelengths are close to the bandgap edges, the effective mode areas of the hybrid PCFs expand quickly, as shown in Fig. 5c(3, 4) and Fig. 5d(3, 4). The effective mode area of the hybrid PCF B is even larger than that of the bandgap PCF at the wavelength of  $1.30\ \mu\text{m}$ , which corresponds to a larger confinement loss than that of the bandgap PCF.

### 3.3 Confinement loss

Figure 6 shows the confinement losses of different PCFs. We can find that the confinement loss of the hybrid PCF A and B are almost between the loss of the index-guiding PCF and the bandgap PCF except at the bandgap edges. The confinement loss of the index-guiding PCF is very low, it increases from  $1.15 \times 10^{-12}$  dB/m at the wavelength  $0.55\ \mu\text{m}$  to  $9.54 \times 10^{-10}$  dB/m at the wavelength  $2.1\ \mu\text{m}$ . For the bandgap PCF, the confinement loss is significantly

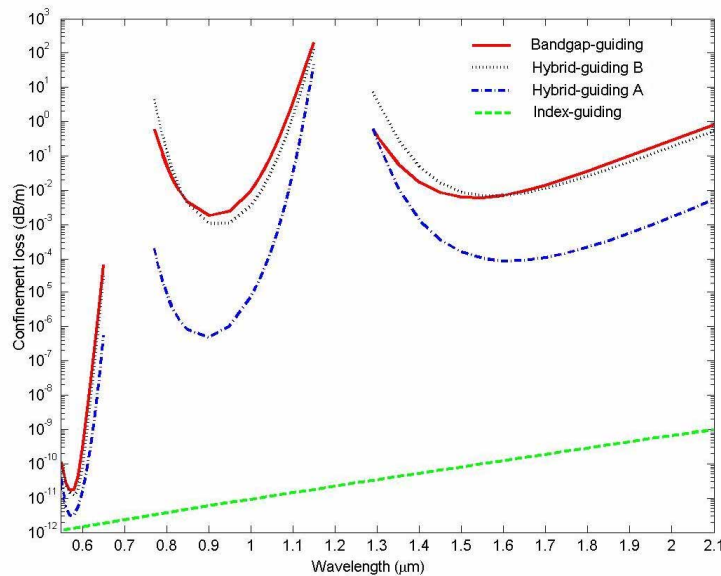


Fig. 6. Confinement loss of the fundamental mode for different fibers as a function of wavelength.

different for all three bandgaps. The confinement loss in the third bandgap is much smaller than the loss in the first and second bandgap. For example, the confinement loss at  $0.58\ \mu\text{m}$  is  $1.75 \times 10^{-11}$  dB/m, however, the confinement losses at  $0.9\ \mu\text{m}$  and  $1.55\ \mu\text{m}$  are respectively

$1.81 \times 10^{-3}$  dB/m and  $6.01 \times 10^{-3}$  dB/m. For the hybrid PCF A, the confinement loss is significantly small because the hybrid fiber structure of A is much closer to that of the index-guiding PCF. For example, the confinement loss at 0.9  $\mu\text{m}$  and 1.55  $\mu\text{m}$  can be improved to  $4.85 \times 10^{-7}$  dB/m and  $1.01 \times 10^{-4}$  dB/m respectively. The improvement of the confinement loss is attributed to the index-guiding part of the hybrid PCF A whose confinement loss is much lower than the bandgap-guiding. It should be noted that it is not for all the cases. For example, when the relative hole size of the index-guiding is significantly small, such as  $d/\Lambda=0.05$ , thus the confinement loss of the index-guiding PCF is larger than the confinement loss of the bandgap PCF, the corresponding hybrid PCF will have lower confinement loss than the index-guiding PCF. So the confinement of the hybrid PCF generally is between the confinement losses of the corresponding index-guiding PCF and bandgap PCF for the operation wavelengths within the middle part of the bandgaps. For the hybrid PCF B, the confinement loss at the short wavelength edge of the bandgap is larger than the bandgap PCF, it may be explained by bandgap theory. The hybrid-PCF B confines light by bandgap effects in the whole cross-section except x direction, the effective index curve is lower than that of bandgap PCF near the short wavelength bandgap edge as shown in Fig. 3, which makes the effective index curve closer to the bandgap edge compared with that of the bandgap PCF or even outside the bandgap, thus causing larger confinement loss.

### 3.4 Group velocity dispersion

The GVD property of a fiber similar to hybrid PCF A has been demonstrated in Ref. [14]. Here we compare the GVD properties of four different PCFs in the first bandgap, as shown in Fig. 7.

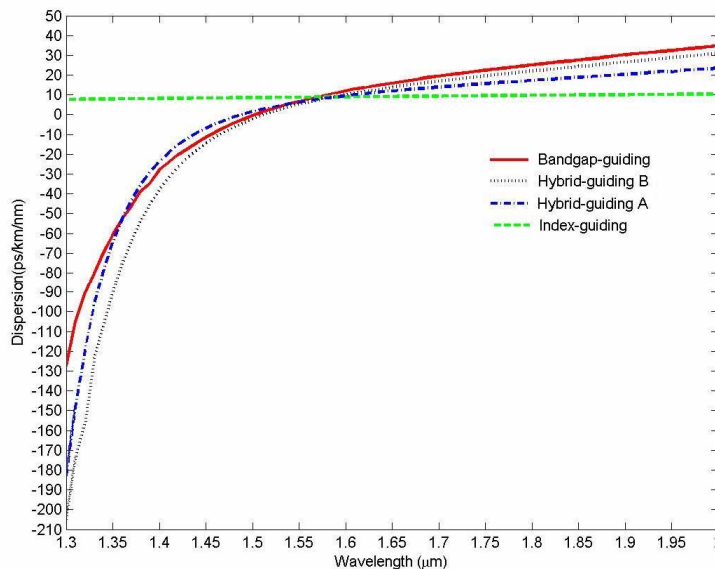


Fig. 7. GVD of the fundamental mode as a function of the wavelength in the first bandgap

The GVD curve shape of hybrid PCF A and B is as similar as that of the bandgap PCF. This is due to the similar effective index properties of the hybrid PCFs and the bandgap PCF caused by the bandgap effect, as shown in Fig. 3. We can find from Fig. 7 that GVD curves of hybrid PCFs, especially hybrid PCF A, are a little bit flattened compared with the bandgap PCF at the center part of the bandgap. However, the GVD curve of the hybrid PCFs becomes more normal when the operation wavelength is near the bandgap edge. Thus the novel

dispersion property of hybrid PCFs can provide new mechanism to design the PCF with modified zero-dispersion wavelength.

### 3.5 Birefringence

Because the guiding mechanisms of the hybrid PCF A and B are different in two orthogonal directions, large birefringence for the hybrid PCF is expected. We calculate the birefringence in the first bandgap, the same property is expected for other bandgaps. To achieve accurate results, we divided one quarter of the fiber cross section into 65280 elements in full-vector FEM. For the index-guiding PCF and the bandgap PCF, the effective index difference of x-polarized and y-polarized fundamental modes which should be degenerate is of the order of  $10^{-7} \sim 10^{-8}$  which is caused by the precision of calculation and could be reduced further by increasing the number of divided elements [18]. Under the same condition, the birefringence of the hybrid PCF A and B is of the order of  $10^{-5}$  as shown in Fig. 8. The birefringence increases with the increase of wavelength, and increases at the short wavelength edge of the bandgap. Thus hybrid PCF has potential to be a high birefringence fiber. For example, when the refractive index and hole diameter of the high-index rod of the hybrid PCF A change to 1.65 and  $6 \mu\text{m}$  respectively, the birefringence of the PCF can be high to  $1.04 \times 10^{-3}$  at the wavelength of  $1.55 \mu\text{m}$ . A more detailed analysis of the high birefringence hybrid PCF will be presented shortly.

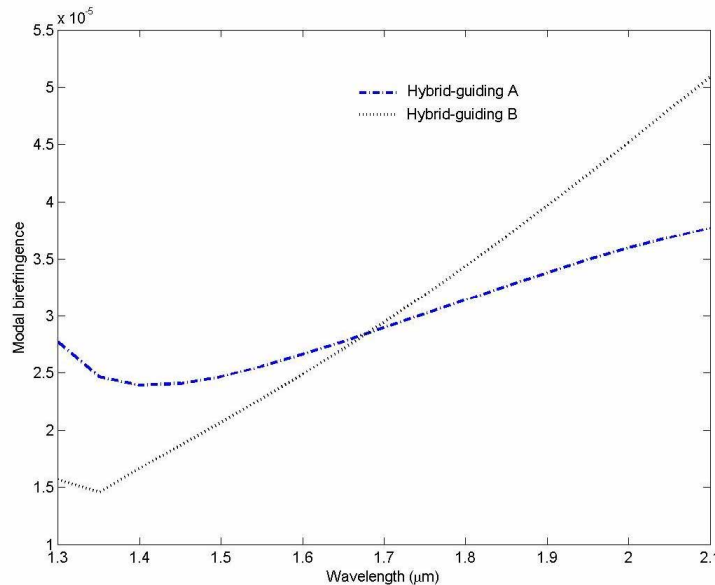


Fig. 8. Birefringence of the fundamental mode as a function of the wavelength in the first bandgap.

## 4. Potential Applications

Because hybrid PCFs have novel guiding mechanism which has the advantages of both index-guiding and bandgap guiding, they have many potential applications. The bending loss of the hybrid PCF A and B in two orthogonal directions are expected to be very different, which may find application as a directional bending sensor. The hybrid PCF can be designed as an ultra-low loss filter or switch compared to bandgap PCFs. Hybrid PCFs provide a new mechanism to design high birefringence PCF and to engineer the dispersion. It can also make novel tunable devices when the high-index rod is replaced by high-index liquid, polymer or liquid crystal by using the selective filling technology introduced in Ref. [23, 24]. This avoids

the complicated and expensive drawing process and allows the modification of the fiber structure and hence various properties. The hybrid PCFs possess a new guiding mechanism which lead us to predict more than three different materials rods can be composed in the fiber and the light can still be well confined in the core, thus providing new ways to design functional fibers such as the fiber composed of semiconductor rods [25, 26], silica and air holes, in which electrons can propagate in the semiconductor rods and photons propagate in the silica core. The combination of hybrid PCF with Bragg gratings and long period gratings may produce grating with new properties, considering that hybrid PCFs may be easier to write gratings using UV light compared with index-guiding PCFs because the index contrast of high-index rod and background silica can be fabricated as low as one percent [27].

## **5. Conclusion**

In conclusion, we have systematically investigated the properties of two hybrid PCFs. The wavelength dependence of the modal effective index, effective mode area, confinement loss, group velocity dispersion and birefringence has been derived by using a simulation model. The properties and advantages of hybrid PCFs are demonstrated by comparing them with those of the corresponding index-guiding PCF and bandgap-guiding PCF. Finally, the potential applications of these hybrid PCFs are discussed.

## **Acknowledgements**

The authors wish to thank Prof. J. C. Knight and Dr. Cerqueira for useful discussion about the gradually index variation model in Ref. [14]. The research work was partly supported by the Hong Kong SAR government through a CERG grant PolyU 5243/04E.